Chapter 5

Investigation of First Order Isostructural Magnetic Transition with a Magnetodielectric Coupling in $0.9BiFeO_3$-$0.1Sr(Fe_{0.5}Nb_{0.5})O_3$ Solid Solution

5.1 Introduction

As discussed in chapter 1, amongst the multiferroic family of compounds, $BiFeO_3$ is a room temperature multiferroic with very high magnetic (T_N ~ 643K) and ferroelectric transition (T_c ~ 1103K) temperatures which continues to attract enormous attention because of its potential for application in room temperature multifunctional devices as novel sensor, actuator and spintronic material [Catalan and Scott (2009), Fiebeg et al. (2005), Gajek et al. (2007), Bibes et al. (2008)]. Recently, an atomic level evidence for linear magnetoelectric (ME) coupling mediated by an isostructural phase transition has been presented in (1-*x*)$BiFeO_3$-*x*$BaTiO_3$ [Singh et al (2008)(C), Singh et al. (2011)] and (1-x)$BiFeO_3$-*x*$Pb(Fe_{0.5}Nb_{0.5})O_3$ [Patel et al. (2013)] systems. A microscopic understanding of the effect of magnetic ordering emerging below T_N ~ 643K, on the already existing ferroelectric order at 643K < T < T_C ~ 1103K in $BiFeO_3$ has been presented only recently, using first principles calculations in conjunction with a spin model [Lee and Fishman (2015)]. This is in marked contrast to type I multiferroics like $TbMnO_3$ with improper ferroelectricity where the spin driven polarization mechanism due to inverse D-M effect [discussed in section 1.4.5 of Chapter 1] is fairly well understood [Kenzelmann (2005), Aoyama et al. (2014)]. Considering various possible microscopic mechanism of ME couplings and spin-driven change in polarization, it has been shown that exchange-striction driven giant polarization (ESP) dominates over other sources of polarization like spin current and single ion anisotropy [Lee and Fishman (2015)]. Further, the ground state of $BiFeO_3$ is still unsettled as a result of the presence of several low temperature weak transitions of magnetic, magnetoelastic and magnetoelectric nature [Catalan and Scott (2009), Ramachandran et al. (2011), Singh et al. (2008)(A)]. One of the magnetic transitions

reported just below room temperature around 250K has been proposed to be either a spin reorientation or spin glass phase transition. Some workers have also reported a strong dielectric relaxation step around this temperature (~ 250K) [Kamba et al. (2007)]. However, both the nature of this transition (spin reorientation or spin glass) and its intrinsic magneto-dielectric nature are not settled.

Results of solid solution formation of $BiFeO_3$ with $Sr(Fe_{0.5}Nb_{0.5})O_3$ discussed in Chapter 4 reveals that a new monoclinic phase in Cc space group appears for the composition range $0.1 \leq x \leq 0.15$. This also breaks the periodicity (~ 62nm) of magnetic cycloid of $BiFeO_3$ giving appreciable non-zero magnetization in the system. Since the monoclinic (Cc) phase is non-centrosymmetric polar as well, one can expect the significant polarization also for such compositions. Thus one can expect multiferroic coupling in the monoclinic compositions of the $(1-x)BiFeO_3$-$xSr(Fe_{0.5}Nb_{0.5})O_3$ solid solution in the composition range $0.1 \leq x \leq 0.15$. It will be interesting, therefore, to investigate the temperature dependent crystal structure, magnetic, dielectric and magnetoelectric and phase transition behaviour of such a composition to develop complete understanding of the structure-property correlations for these compositions. In view of this, we have selected the composition with x=0.10 of $(1-x)BiFeO_3$-$xSr(Fe_{0.5}Nb_{0.5})O_3$ solid solution to investigate in detail. This chapter presents the results of temperature dependent crystal structure, magnetization, M-H hysteresis, dielectric, and magnetoelastic and phase transition studies on the composition with x=0.10.

We present experimental evidence for the existence of a robust first order isostructural magnetic transition at 255K that is accompanied with magnetoelastic coupling and an intrinsic magnetodielectric relaxation step, with a negative linear magnetodielectric coupling. Below this magnetic transition, the step like variation of unit cell volume and unit cell parameters as a function of temperature reveal two more

anomalies where different kind of phase transitions (such as magnetic, glassy, magnetoelastic, spin reorientation and magnetoelectric) have been reported in $BiFeO_3$ ceramic/single crystal [Scott et al. (2008), Singh et al. (2008)(B), Ramachandran et al. (2009), Redfern et al. (2008)]. The results are supported by dc magnetization M(T), ac magnetic susceptibility $\chi(\omega, T)$, dielectric and structural studies below room temperature.

5.2 Experimental

Sintered powder sample of phase pure $0.90BiFeO_3$-$0.10Sr(Fe_{0.5}Nb_{0.5})O_3$ (0.90BF-0.10SFN) was prepared by conventional solid state reaction approach, the details of which are already described in Chapter 2. Sintered pellets were crushed into fine powder and annealed at 773 K for 10 hours to remove the strains introduced during crushing. The annealed powder was used for the collection of temperature dependent x-ray diffraction patterns in the temperature range 12K-300K during heating in 2θ range 20^o to 120^o at a step of 0.02^o. The XRD data was collected using an 18 kW rotating anode (CuK_α) based Rigaku powder diffractometer (D/Max-2500/PC series) operating in Bragg-Brentano geometry with curved crystal monochromator in the diffracted beam. The cooling of sample was done by He-cryostat based attachment on the same diffractometer. For dielectric measurements, the sintered pellets of 0.90BF-0.10SFN ceramic were gently polished with 0.25μm diamond paste for about 4-5 minutes and then washed with acetone to clean the surface. Isopropyl alcohol was then applied to the polished surface for removing the moisture, if any, on the pellet surfaces and then fired. Silver paste was applied on both the surfaces of the fired pellets. It was first dried at 373K in an oven and then fired again in a furnace at 773K about 5 minutes. The dielectric permittivity (ε_r) and loss tangent ($\tan\delta$) in the temperature range 2K to 300K of silver electroded pellets were measured with and without the application of magnetic

field using Cryogen free Superconducting Magnet and Nova Control (alpha-A) high performance frequency analyser. The temperature dependent dc magnetisation M(T) at a measuring field of 500 Oe, in the formalism of zero-field cooled (ZFC), field-cooled cooling (FCC) and field-cooled warming (FCW), magnetisation versus magnetic field (M-H loop) and ac magnetic susceptibility $\chi(\omega, T)$ measurements were carried out in the temperature range of 2K to 300K using a Quantum Design MPMS-3 system based on SQUID sensor.

5.3 Results and Discussion

5.3.1 Temperature Dependence of dc Magnetization M(T) for $0.90BiFeO_3$-$0.10Sr(Fe_{0.5}Nb_{0.5})O_3$ Ceramic

Temperature dependence of dc-magnetization M(T) for 0.90BF-0.10SFN ceramic is shown in Fig. 5.1. As can be seen from Fig. 5.1, a clear magnetic transition is present around 255K and the FCC and FCW measured data exhibit thermal hysteresis. It indicates the first order characteristic of this magnetic transition around 255K. As we go from room temperature towards low temperature side we observe that up to temperature of ~ 100K, the value of magnetisation decreases with temperature as expected for a conventional antiferromagnetic material. However, no clear signature of another magnetic transition is observed in contrast to pure $BiFeO_3$. In pure $BiFeO_3$, Scott et.al have reported two magnetic phase transitions below room temperature at 140K and 200K and both are interpreted as spin-reorientation transitions [Scott et al. (2008)]. It has been reported that, at room temperature the magnetic moment of Fe^{3+} ions are confined in the (-12-1) plane of the cycloid [Cazayous et al (2008)]. The temperature dependence of the Raman integrated intensities of the electromagnon for $BiFeO_3$ exhibit a maximum around 140K which is attributed to small reorientation of spin out of the cycloid plane [Cazayous et al (2008)].

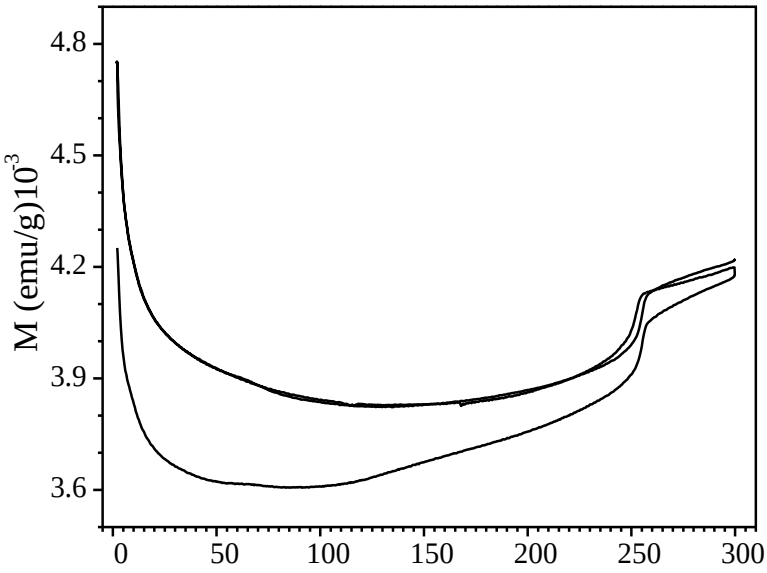

Figure 5.1 Temperature dependence of ZFC, FCC and FCW magnetization for 0.90BF-0.10SFN ceramic.

In order to study the temperature dependent behaviour of remanent magnetization (M_r) and coercive field (H_c), M-H hysteresis loops were measured at various temperatures under applied magnetic field up to ± 60kOe. The temperature dependence of M-H hysteresis loops in the temperature range 300K to 25K at 25K interval is shown in Fig. 5.2 (a). One can clearly see that all the M-H loops are open and the value of remnant magnetization and coercive field is changing by changing the temperature. In Fig 5.2(b) and (c) we present the temperature dependence of coercive field (H_c) and remnant magnetisation (M_r). The value of coercive field (H_c) first increases from room temperature up to 250K, then decreases (softening) from temperature 250K up to 150K and then further starts increasing (hardening) up to 25K. This trend and variation of H_c leads to two anomalies at 150K and 250K indicating presence of magnetic phase transition around these temperatures. The 250K temperature is in fact very close to 255K magnetic transition temperature observed from M(T) measurement. Further the temperature dependence of remanent magnetization (M_r) given in Fig 5.2(c) also shows a minimum around 140K suggesting some magnetic

transition around this temperature. As discussed in next section, there are two magnetoelastic transitions below room temperature around 255K and 145K. Now we will confirm this using low temperature XRD study.

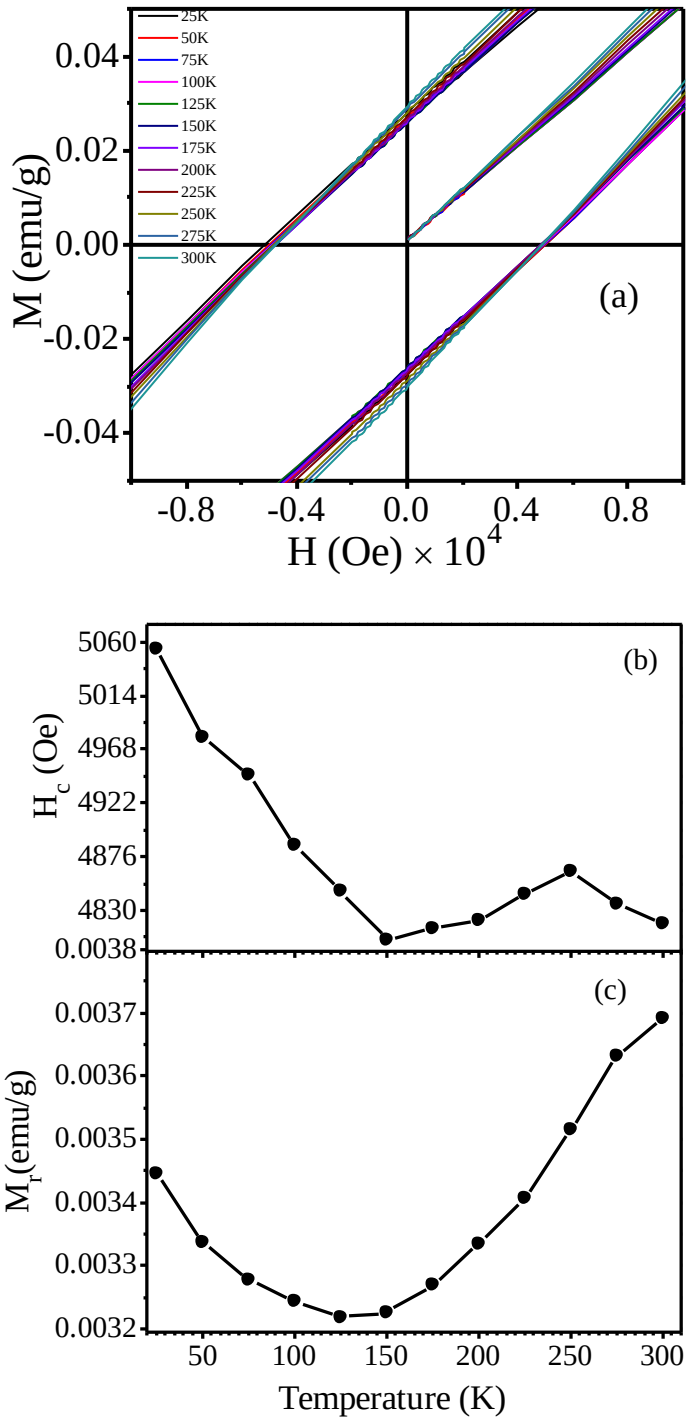

Figure 5.2 Temperature dependence of (a) M-H hysteresis loop (b) coercive field H_c (c) remnant magnetization M_r for 0.90BF-0.10SFN ceramic.

5.3.2 Study of Magnetoelastic Coupling in 0.90BF-0.10SFN ceramic: XRD Analysis

To investigate the magnetoelastic transitions in 0.90BF-0.10SFN ceramic and correlation of low temperature magnetic transitions with crystal lattice, we performed low temperature XRD studies. The x-ray powder diffraction patterns of 0.90BF-0.10SFN ceramic were collected in the temperature range of 12K to 300K in a heating mode of measurement. The stacking of superlattice reflections and pseudocubic (222), (400) and (440) (all indices taken with respect to double cubic perovskite cell) profiles peaks of raw XRD data at some selected temperatures is depicted in Fig. 5.3. As can be seen from this figure, the shape of the XRD profile peaks remain unchanged except a small shift towards lower 2θ side as we go in higher temperature region. There is no additional peak splitting or disappearance of any XRD peak on changing temperature. This reveals that the crystal structure of 0.90BF-0.10SFN ceramic does not change in this temperature range below room temperature. In view of this, the crystal structures at various temperatures were successfully refined by Rietveld technique using monoclinic model with *Cc* space group. After successful structure refinement at various temperatures, we present the full pattern Rietveld fits of X-ray powder diffraction patterns at some selected temperatures namely 300K, 200K, 160K, and 12K in Fig.5.4. The continuous overlapping line (black), dots (red) and the bottom line (blue) profiles represent Rietveld calculated, experimentally observed and difference XRD patterns, respectively, obtained from Rietveld refinement. The vertical bars (magenta) show Bragg's peak positions. The Rietveld fits of 222, 400 and 440 profiles at some representative temperatures like 300K, 200K, 100K and 12K were depicted in Fig. 5.5 to illustrate the quality of fits. Very good fits confirm the *Cc* space group for 0.90BF-0.10SFN ceramic in the temperature range 12K to 300K shows that the monoclinic phase remains stable in the temperature range between 12K and 300K.

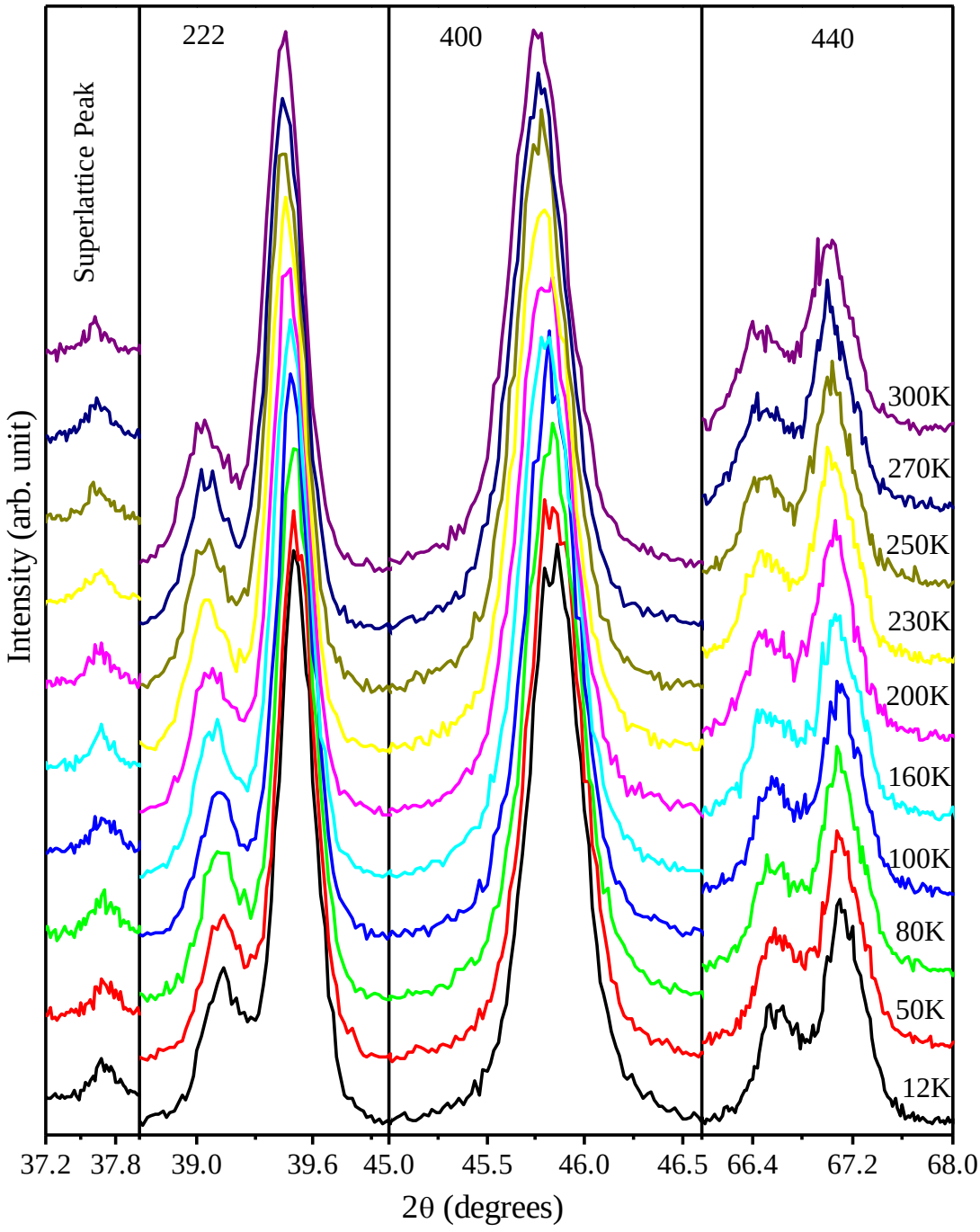

Figure 5.3 Evolution of the XRD profiles of pseudocubic perovskite peaks (222), (400) and (440) and superlattice reflection at some selected temperatures 12, 50, 80, 100, 160, 200, 230, 250, 270 and 300 K for 0.90BF-0.10SFN ceramic, showing the absence of any crystallographic phase transition.

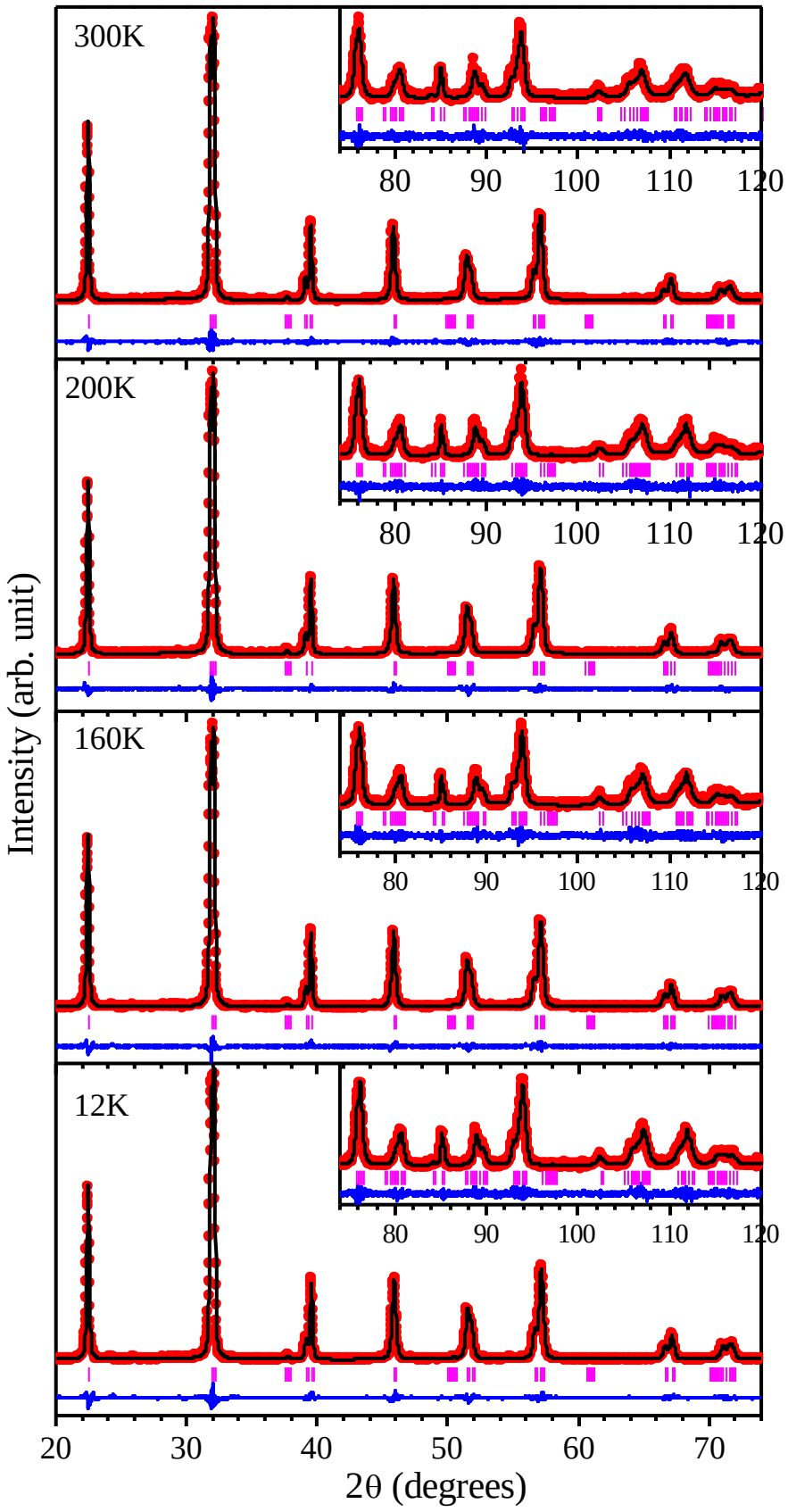

Figure 5.4 The experimentally observed (dots), Rietveld calculated (overlapping continuous plot), and difference (bottom curve) XRD profiles for $0.9BiFeO_3$-$0.10Sr(Fe_{0.5}Nb_{0.5})O_3$ ceramic at various temperatures using *Cc* space group.

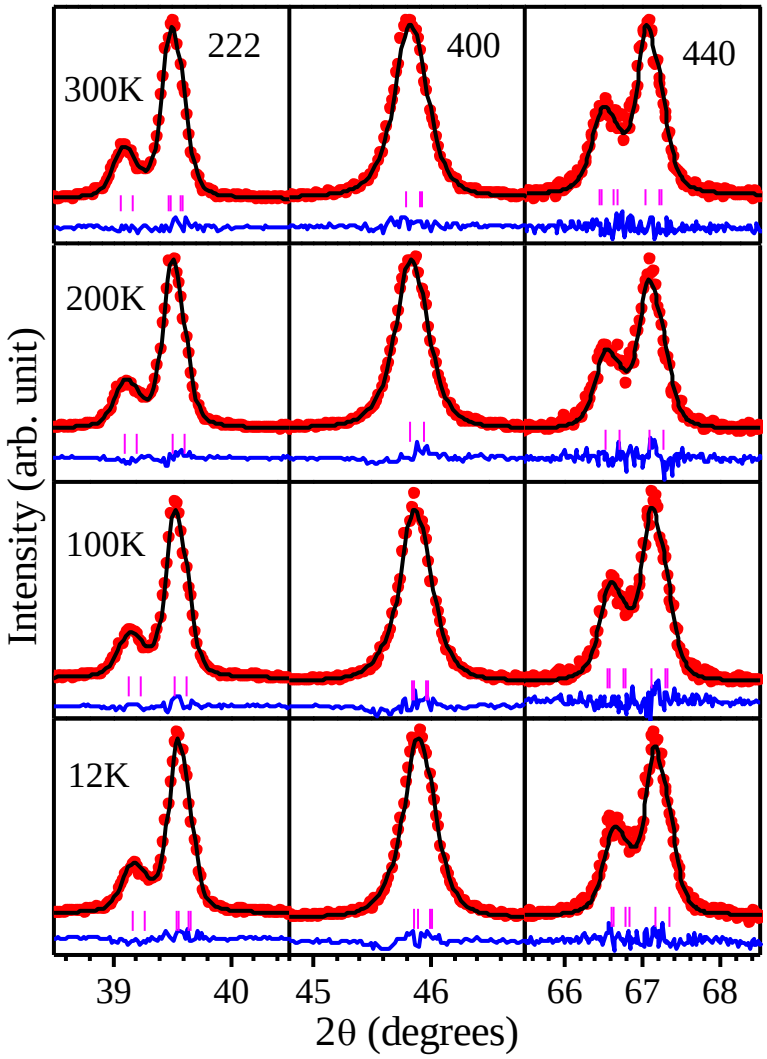

Figure 5.5 The experimentally observed (dots), Rietveld calculated (overlapping continuous plot), and difference (bottom curve) XRD profiles of pseudocubic perovskite peaks (222), (400) and (440) for 0.90BF-0.10SFN ceramic at temperatures 300K, 200K, 100K and 12K.

The Rietveld refined structural parameters are given in Table 5.1. While there is no crystallographic phase transition in 0.90BF-0.10SFN ceramic below room temperature, the unit cell volume obtained from Rietveld structure refinement at various temperatures exhibits step like changes with temperature as shown in Fig. 5.6(a).

Table 5.1 Rietveld refined structural parameters for $0.9BiFeO_3$-$0.1Sr(Fe_{0.5}Nb_{0.5})O_3$ ceramic sing the monoclinic phase with *Cc* space group.

Space group: *Cc*				
	250K	200K	160K	12K
a (Å)	9.7574(3)	9.7538(3)	9.7507(3)	9.7422(3)
b (Å)	5.5778(3)	5.5764(3)	5.5750(3)	5.5720(3)
c (Å)	5.6222(4)	5.6206(3)	5.6183(4)	5.6133(4)
$Bi^{+3}/Sr^{+2}x$	0.00	0.00	0.00	0.0
$Bi^{+3}/Sr^{+2}y$	0.25	0.25	0.25	0.25
$Bi^{+3}/Sr^{+2}z$	0.0	0.0	0.0	0.0
$Fe^{+3}/Nb^{+5}x$	0.2289(15)	0.2282(15)	0.2293(14)	0.2300(13)
$Fe^{+3}/Nb^{+5}y$	0.2371(15)	0.2366(14)	0.2371(15)	0.2364(12)
$Fe^{+3}/Nb^{+5}z$	0.789(3)	0.788(3)	0.791(3)	0.792(3)
$O^{-2}1x$	-0.032(6)	-0.028(5)	-0.030(6)	-0.030(5)
$O^{-2}1y$	0.200(10)	0.192(12)	0.194(12)	0.182(15)
$O^{-2}1z$	0.589(9)	0.589(8)	0.584(9)	0.575(9)
$O^{-2}2x$	0.195(5)	0.191(6)	0.192 (5)	0.191(6)
$O^{-2}2y$	0.539(9)	0.527(16)	0.530(13)	0.521(16)
$O^{-2}2z$	-0.004(12)	0.001(15)	0.000(13)	0.012(14)
$O^{-2}3x$	0.243(8)	0.247(8)	0.245(8)	0.249(6)
$O^{-2}3y$	0.038(14)	0.033(14)	0.041(13)	0.034(13)
$O^{-2}3z$	0.114(13)	0.124(11)	0.120(12)	0.128(11)
χ^2	1.26	1.22	1.31	1.39
β	125.763(3)	125.759(3)	125.752(3)	125.734(3)

It is evident from Fig. 5.6(a) that, as we go below room temperature, we see that the unit cell volume start decreasing up to 260K with constant slope and then a change occurs in it at this temperature that marks an anomaly around 250K. This type of change in slope is also observed around 150K and 40K that leads to two more anomalies. These anomalies in temperature dependent variation of unit cell volume are marked by arrows in Fig. 5.6(a). Thus the magnetic measurements and temperature variation of unit cell volume suggests the presence of two magnetoelastic transitions at 255K and 150K. To confirm it further, we have studied the temperature dependent variation of monoclinic unit cell parameters i.e. a, b, c and monoclinic distortion angle (β) as depicted in Fig. 5.7. The temperature dependent variation of cell parameters also have step like variation at the temperatures where anomaly is observed in the unit cell volume. The appearance of anomaly in the cell parameters (a, b, c and β) and unit cell volume at magnetic transition temperature 255K directly confirms the presence of magnetoelastic coupling in the magnetically ordered phase for $0.90BiFeO_3$-$0.10Sr(Fe_{0.5}Nb_{0.5})O_3$ ceramic.

The variation of static permittivity ε_{rs} (0T), (here '0T' stands for zero Tesla i.e. the absence of external applied magnetic field) calculated from Cole-Cole technique (discussed in details in section 5.3.4), as a function of temperature is shown in Fig. 5.6(b). It also shows a step like variation around the magnetic transition temperature 255K. The value of ε_{rs}(0T) varies linearly in the temperature range 230K to 267K. Further, in Fig. 5.6(c) we present the temperature dependent variation of ac magnetic susceptibility $\chi(\omega, T)$ measured at frequencies 97, 297, and 497 Hz to investigate the nature of magnetic transitions in $0.9BiFeO_3$-$0.1Sr(Fe_{0.5}Nb_{0.5})O_3$ ceramic. There is no signature of the spin glass like behaviour except around 30K where a peak is seen in the ac magnetic susceptibility $\chi(\omega, T)$. Thus our experimental results depicted in Fig. 5.6

and Fig. 5.1 rule out any possibility of spin glass transition at 255K. In fact these results strongly support the existence of a first order isostructural magnetic transition which is accompanied with magnetoelastic coupling. As shown in the subsequent sections (5.3.3 and 5.3.4), at 255K, there is an intrinsic magnetodielectric step, with negative linear magnetodielectric coupling (see Fig. 5.10).

In pure $BiFeO_3$, an antiferromagnetic to spin reorientation transition has been reported around (140-150K) [Scott et al. (2008), Singh et al. (2008)(B), Ramachandran et al. (2009), Redfern et al. (2008)]. A magnetic transition of glassy nature but with the feature of magnetoelectric coupling is also reported around (38-50K) in $BiFeO_3$ [Singh et al. (2008)(B), Ramachandran et al. (2009), Redfern et al. (2008)]. Our experimental results on $0.90BiFeO_3$-$0.10Sr(Fe_{0.5}Nb_{0.5})O_3$ strongly suggest the presence of a weak magnetoelastic coupling at 145K which is very close to the temperature (140-150K) where an antiferromagnetic to spin reorientation transition in $BiFeO_3$ has been reported by earlier workers [Scott et al. (2008), Singh et al. (2008)(B), Ramachandran et al. (2009), Redfern et al. (2008)]. The peaks observed at 30K in the ac magnetic susceptibility $\chi(\omega,T)$ measurement (Fig. 5.6(c)) shows frequency dispersion and is very close to the reported spin glass freezing temperature (29.4K) in $BiFeO_3$ single crystal [Singh et al. (2008)B]. Thus we may conclude that, the two anomalies around 145K and 40K as appeared in the temperature dependent variation of unit cell volume as well as lattice parameters correspond to the spin glass like behaviour which is also confirmed from the ac susceptibility $\chi(\omega, T)$ measurement. Further, the anomaly in unit cell volume at spin glass transition indicates the presence of magnetoelastic coupling also.

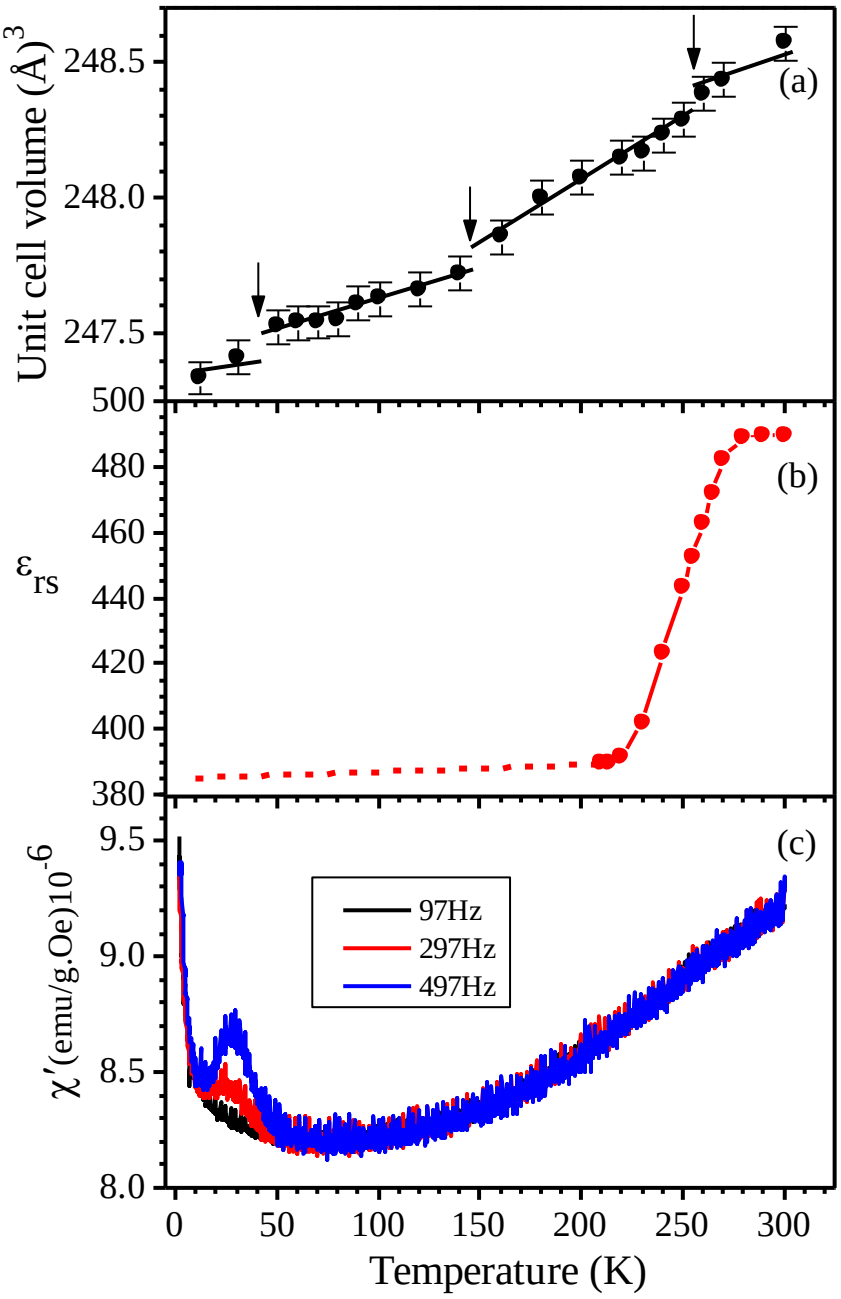

Figure 5.6 Temperature dependent variation of (a) unit cell volume (V), arrows indicate the temperature at which unit cell volume shows anomaly (b) static permittivity (dielectric permittivity in the limit $\omega \rightarrow 0$), where dots are experimental data and dotted line shows extrapolation in the lower temperature region and (c) magnetic ac susceptibility $\chi(\omega, T)$, for $0.90BiFeO_3$-$0.10Sr(Fe_{0.5}Nb_{0.5})O_3$ ceramic.

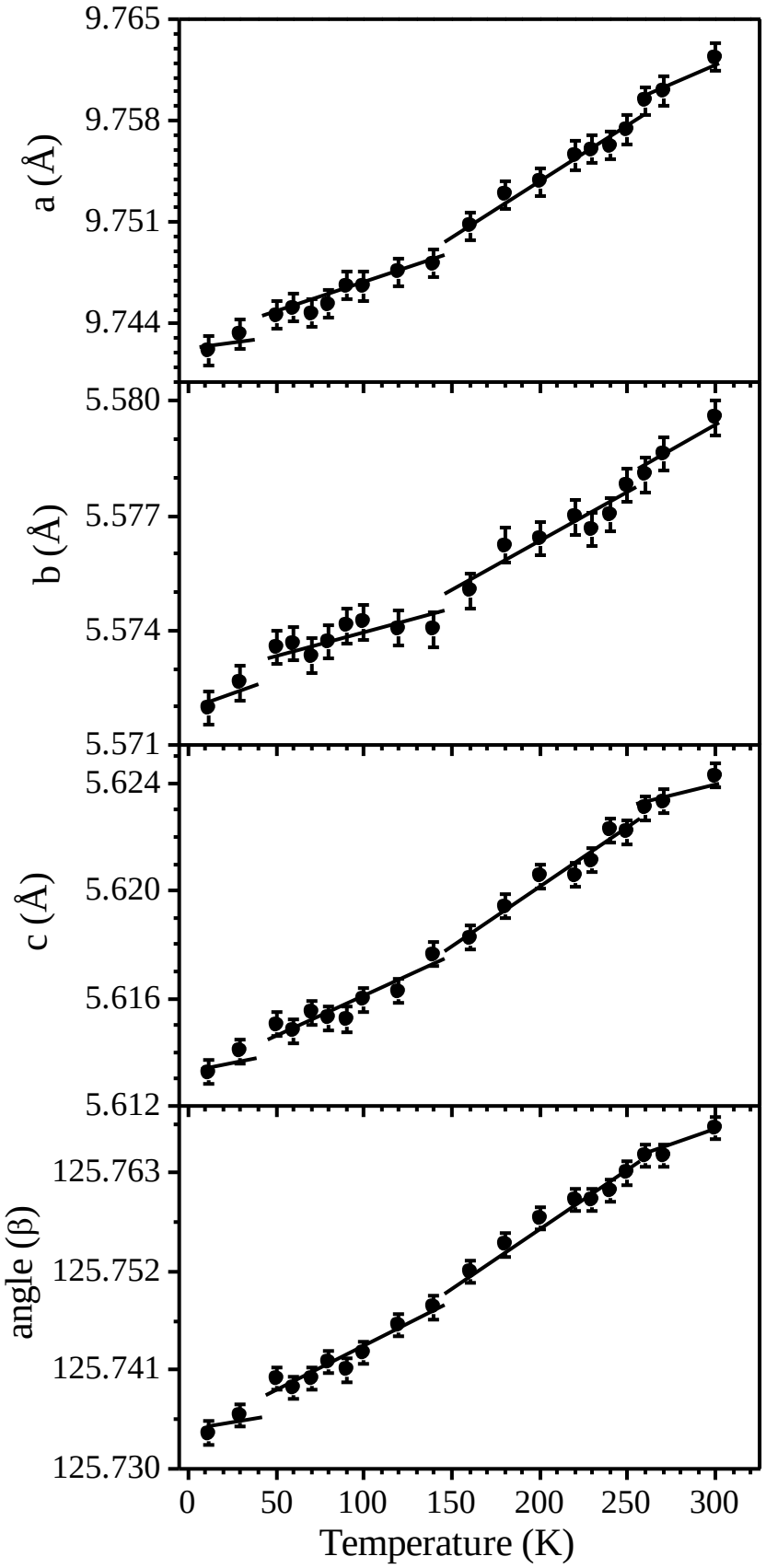

Figure 5.7 Temperature dependent variation of monoclinic (*Cc*) unit cell parameters *a*, *b*, *c* and angle (β) (in degrees) for $0.90BiFeO_3$-$0.10Sr(Fe_{0.5}Nb_{0.5})O_3$ ceramic.

5.3.3. Temperature Dependent Dielectric Behaviour of $0.90BiFeO_3$-$0.10Sr(Fe_{0.5}Nb_{0.5})O_3$ Ceramic

Fig. 5.8 shows the temperature dependent variation of real $\varepsilon'_r(T)$ and imaginary $\varepsilon''_r(T)$ parts of the dielectric permittivity of 0.90BF-0.10SFN ceramic in the temperature range 2K to 315K at various frequencies in the 600Hz to 300kHz. A giant dielectric relaxation step, similar to that reported in $CaCu_3Ti_4O_{12}$ [Subramanian et al. (2000)], $Ba(Fe_{0.5}Nb_{0.5})O_3$ [Saha and Sinha (2002)(A)], $Sr(Fe_{0.5}Nb_{0.5})O_3$ [Raevski et al. (2003)] and $Ba(Fe_{0.5}Ta_{0.5})O_3$ [Raevski et al. (2003)], is clearly observed in the low temperature region. The remarkable feature of the temperature dependence of permittivity is that the value of ε_r' is nearly dispersion-less and temperature independent below ~ 180K with values in the range 50-64. A slight increase in the value of ε_r' from 50 to 64 on heating may be due to phonon softening that leads to significant increase of ε_r' above ~ 195K giving rise to a giant dielectric relaxation step. This relaxation step shifts towards higher temperatures as frequency increases. In $BiFeO_3$ ceramics, this type of low temperature giant dielectric relaxation step was reported by Kamba et al. (2007) and authors attributed the origin of such giant dielectric relaxation to Maxwell-Wagner-type contribution to the permittivity as a consequence of increased conductivity of the grains as compared to the grain boundaries [Singh et al. (2008C)]. Similar relaxation steps have also been reported in $Sr(Fe_{0.5}Nb_{0.5})O_3$ [Liu et al. (2007)] ceramic around 250K and 450K. They found that low temperature relaxation step was not sensitive to thermal treatment in O_2 atmosphere, while that corresponding to high temperature was very sensitive to it. They also reported that the low temperature relaxation step follow Arrhenius law with activation energy equal to 0.38eV and is caused by thermally induce electronic process.

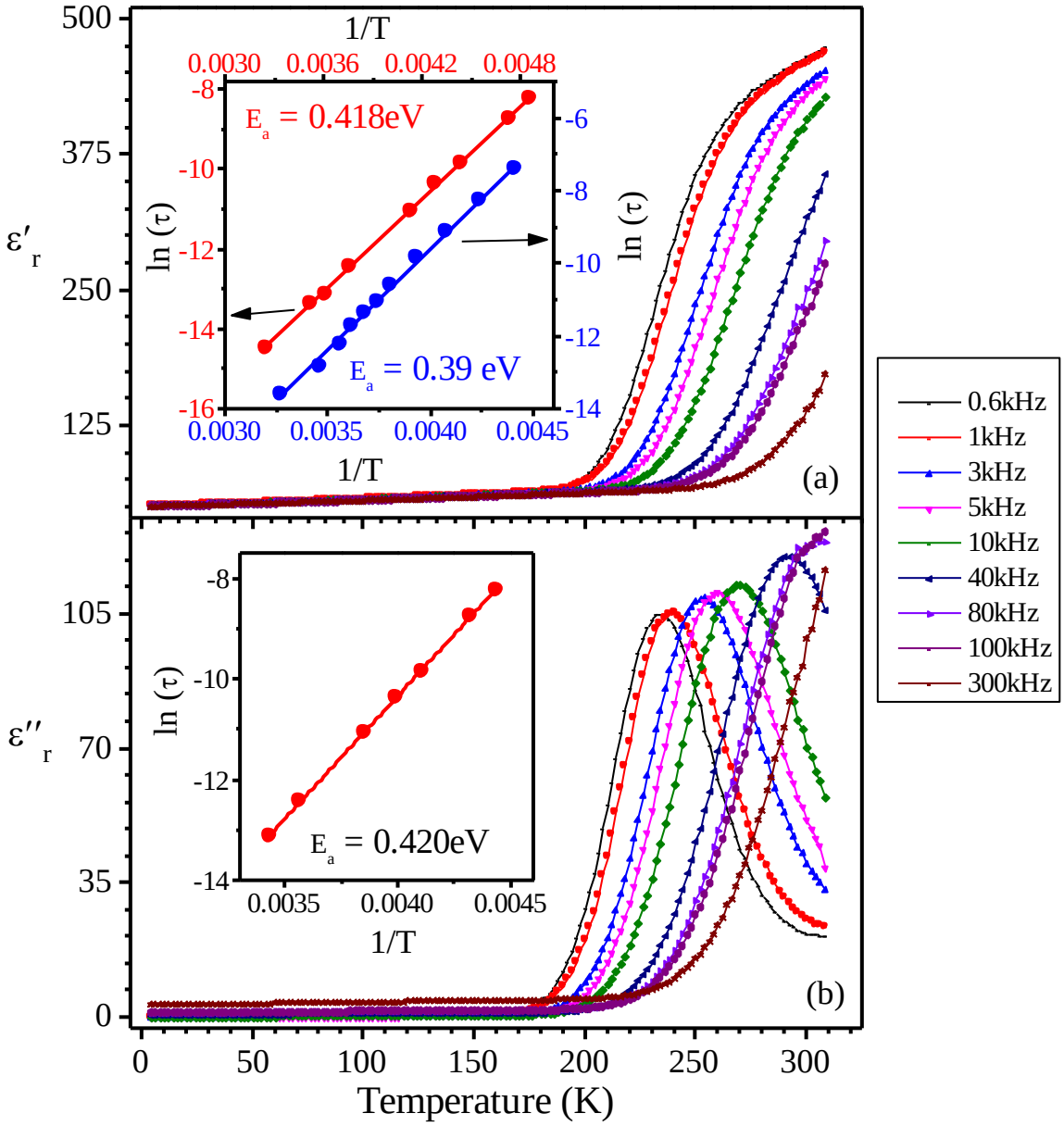

Figure 5.8 Temperature dependence of (a) real part $\varepsilon_r'(T)$ and (b) imaginary part $\varepsilon_r''(T)$ of dielectric permittivity. The insets of (a) and (b) represent corresponding Arrhenius fits for $0.90BiFeO_3$-$0.10Sr(Fe_{0.5}Nb_{0.5})O_3$ ceramic. The data points and activation energy (E_a) shown in the inset (a) (in blue colour) are calculated from Cole-Cole analysis. The symbols, in each inset, are experimental data and solid lines are the least square fits.

To examine the intrinsic/extrinsic origin of giant dielectric relaxation step in $0.90BiFeO_3$-$0.10Sr(Fe_{0.5}Nb_{0.5})O_3$ ceramic, we have performed Cole-Cole analysis and studied the variation of relaxation time with temperature using the real and imaginary

part of dielectric data. As shown in the inset of Fig. 5.8 (a and b), the variation of relaxation time obeys the Arrhenius law,

$$\tau = \tau_0 \exp(E_a/kT)$$

Where, τ_0 is the pre-exponential factor, E_a is the activation energy and k is the Boltzmann's constant. We have fitted real and imaginary part of permittivity data of $0.90BiFeO_3$-$0.10Sr(Fe_{0.5}Nb_{0.5})O_3$ ceramics separately using Arrhenius law as shown in the inset to Fig. 5.8(a) and 5.8(b) respectively. We have also calculated activation energy (E_a) using the data extracted from Cole-Cole analysis (discussed in the next section) and Arrhenius law as shown in the inset of Fig. 5.8(a) (blue colour). The values of activation energy (E_a) as calculated by Arrhenius fitting of experimental data of real and imaginary parts of dielectric permittivity and Cole-Cole analysis are 0.418eV, 0.420eV and 0.39eV, respectively. These values are very close to each other. The closer values of activation energies calculated by these formalisms (real, imaginary part of dielectric permittivity and Cole-Cole analysis) indicate toward the intrinsic origin of giant dielectric relaxation step in the present study.

5.3.4. Low Temperature Cole-Cole Analysis: Observation of a Negative Linear Magnetodielectric Coupling

We have carried out Cole-Cole analysis in the low temperature region of 0.90BF-0.10SFN dielectric data to separate out intrinsic permittivity value from extrinsic one. For Cole-Cole plot, we have taken out data from frequency range 42Hz to 1MHz at temperatures 300K, 280K, 270K, 265K, 260K, 255K, 250K, 240K, 230K, 220K and 210K. We needed to fit two semicircles touching together from temperature 300K to 250K and below this temperature only one semicircle is needed. The Cole-Cole analysis fits at four different temperatures is shown in Fig. 5.9. As we go towards low

temperature side the semicircle belonging to the low frequency side start to disappear and only one semicircle remains at and below 240K.

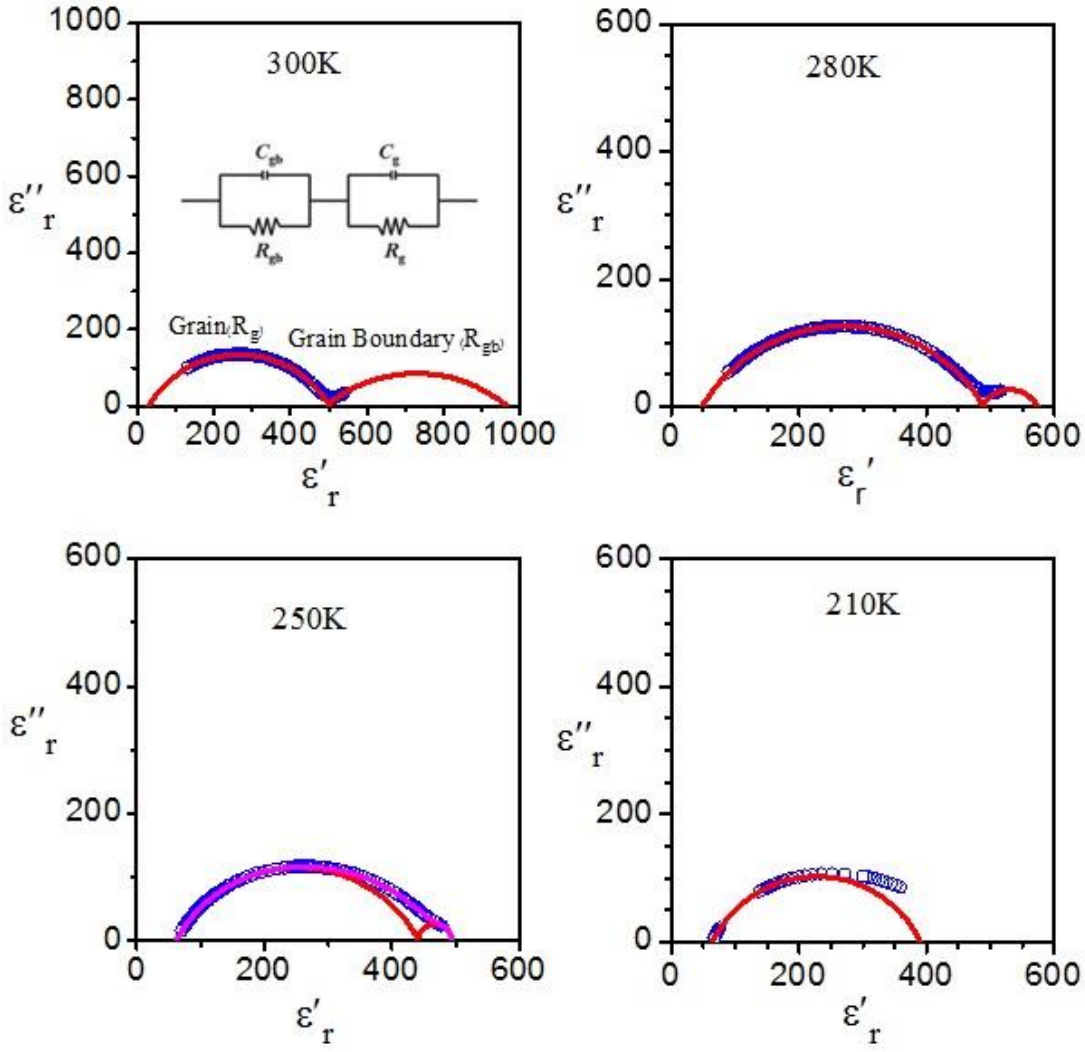

Figure 5.9 Cole-Cole analysis plots for permittivity at four different temperatures in the absence of magnetic field for $0.90BiFeO_3$-$0.10Sr(Fe_{0.5}Nb_{0.5})O_3$ ceramic. Open circles (blue) are data points and continuous curve (red) is the fitted circle. Inset to the Cole-Cole plot at 300 K shows schematic diagram of R-C elements.

As we know that there are three contributions to the dielectric permittivity, one from grain electrode interface, second grain-grain interface and third from grains. Thus in order to separate out the intrinsic dielectric permittivity of 0.90BF-0.10SFN, contributions from the grain boundaries and the electrodes need to be subtracted from

the measured value. Since the contributions from the grain boundaries and the electrode persists in the frequency range of a few Hz to few kHz only, therefore the dielectric constant obtained above this frequency range will give the intrinsic value to the dielectric permittivity (grain contributions only) of the material. For Cole-Cole analysis we have plotted imaginary part of dielectric permittivity against real part which follows the empirical relation [Kao (2004)]:

$$\varepsilon_r^* - \varepsilon_\infty = \frac{\varepsilon_{rs} - \epsilon_\infty}{1 + (j\omega\tau)^{1-\alpha}}$$

Where ε_{rs} and ε_∞ represent dielectric constant measured at very low frequency ($\omega \rightarrow 0$) and very high frequency respectively (i.e. the two ends of semicircle where it meet the real axis, the left end corresponds to very high and the right end to the very low frequency), 'j' is imaginary number $\sqrt{-1}$. 'ω' is the angular frequency of the applied electric field, 'τ' is the relaxation time and 'α' is the parameter having value $0 < \alpha < 1$. The semicircle fitted using above equation has centre at

$$\left[\frac{\varepsilon_{rs} - \varepsilon_\infty}{2}, -\left(\frac{\varepsilon_{rs} - \varepsilon_\infty}{2}\right)\tan\frac{\pi\alpha}{2}\right]$$

The temperature dependence of static permittivity $\varepsilon_{rs}(0T)$ (here '0T' stands for zero Tesla i.e. the absence of external applied magnetic field) is already presented in Fig. 5.6(b). The value of $\varepsilon_{rs}(0T)$ varies linearly in temperature range 230K to 267K and above this range it is nearly temperature independent. Within the limits of experimental errors it is very similar to the giant dielectric relaxation steps as observed experimentally in dielectric measurement and supports to its intrinsic origin.

For the study of magnetodielectric coupling, we carried out low temperature dielectric measurement in the presence of external magnetic field of 3 Tesla in magnitude. After collection of dielectric data, we have performed again Cole-Cole analysis as earlier and determined the values of $\varepsilon_{rs}(3T)$. The percentage change in the

static value of dielectric permittivity due to magnetic field (magnetodielectric response) was calculated using the expression

$$\frac{\varepsilon_{rs}(3\mathrm{T}) - \varepsilon_{rs}(0\mathrm{T})}{\varepsilon_{rs}(0\mathrm{T})} * 100$$

where, $\varepsilon_{rs}(0\mathrm{T})$ represents the value of static dielectric permittivity in the absence of magnetic field. In Fig. 5.10, we have plotted the temperature dependent variation of percentage change in the value of permittivity on the application of magnetic field of 3 Tesla (magnetodielectric response). We see that, it first shows negative but linear increase and mark a peak around temperature 250K which is very close to the observed magnetic phase transition in M(T). This experimental observation provides confirmatory evidence for the possibility of negative linear magnetodielectric coupling in the present ceramic.

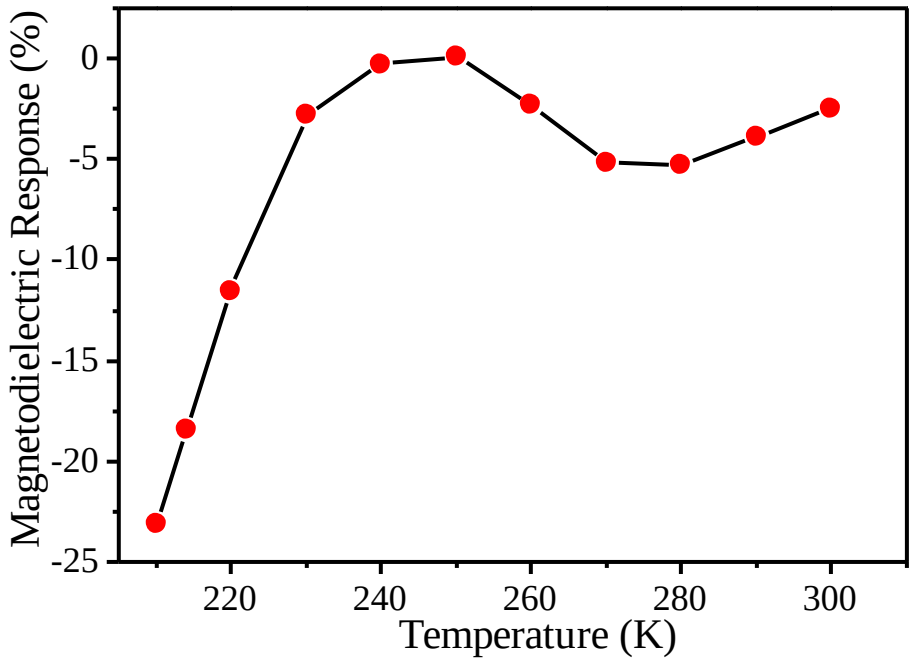

Figure 5.10 Temperature dependence of Magnetodielectric response calculated from static dielectric permittivity (ε_{rs}) for $0.90BiFeO_3$-$0.10Sr(Fe_{0.5}Nb_{0.5})O_3$ ceramic.

5.4 Conclusions

We have presented the room temperature crystal structure of $0.9BiFeO_3$–$0.1Sr(Fe_{0.5}Nb_{0.5})O_3$ ceramic using high resolution X-ray diffraction data. It has been found that the substitution of 10% $Sr(Fe_{0.5}Nb_{0.5})O_3$ in $BiFeO_3$ lead to a structural transformation from pre-existing rhombohedral structure of $BiFeO_3$ in *R*3*c* space group to monoclinic structure in *Cc* space group. The Rietveld analysis of temperature dependent x-ray powder diffraction data at various temperatures exhibits three anomalies in the unit cell volume and lattice parameters. All anomalies are found to be isostructural. Out of three anomalies two are observed in dc magnetization M(T) measurement: the first anomaly appeared at 255K with robust nature and the second one appeared as a broad hump around 145K. These two anomalies in M(T) is also supported by temperature variation of coercive field (H_c). Our experimental results on structural, dielectric and ac susceptibility $\chi(\omega,T)$ ruled out the possibility of spin glass transition at 255K [Ramachandran et al. (2009)] and support the existence of a first order isostructural magnetic transition that is accompanied with magnetoelastic coupling and an intrinsic magnetodielectric relaxation step, with a negative linear magnetodielectric coupling. Further, the second anomaly in M(T) and structural results support the presence of weak magnetoelastic coupling at 145K where a spin reorientation transition [Scott et al. (2008), Singh et al. (2008)(B), Ramachandran et al. (2009), Redfern et al. (2008)] also reported. The last anomaly appearing in unit cell volume and lattice parameters around 40K is very close to the peaks appeared in magnetic ac susceptibility measurement. This shows that the transition around 40K has glassy nature with the presence of magnetoelastic effect.